Exploring changes in the spatial distribution of stream baseflow generation during a seasonal recession

R. A. Payn,[1,2] M. N. Gooseff,[3] B. L. McGlynn,[2] K. E. Bencala,[4] and S. M. Wondzell[5]

[1]   Relating watershed structure to streamflow generation is a primary focus of hydrology. However, comparisons of longitudinal variability in stream discharge with adjacent valley structure have been rare, resulting in poor understanding of the distribution of the hydrologic mechanisms that cause variability in streamflow generation along valleys. This study explores detailed surveys of stream base flow across a gauged, 23 km^2 mountain watershed. Research objectives were (1) to relate spatial variability in base flow to fundamental elements of watershed structure, primarily topographic contributing area, and (2) to assess temporal changes in the spatial patterns of those relationships during a seasonal base flow recession. We analyzed spatiotemporal variability in base flow using (1) summer hydrographs at the study watershed outlet and 5 subwatershed outlets and (2) longitudinal series of discharge measurements every ~100 m along the streams of the 3 largest subwatersheds (1200 to 2600 m in valley length), repeated 2 to 3 times during base flow recession. Reaches within valley segments of 300 to 1200 m in length tended to demonstrate similar streamflow generation characteristics. Locations of transitions between these segments were consistent throughout the recession, and tended to be collocated with abrupt longitudinal transitions in valley slope or hillslope-riparian characteristics. Both within and among subwatersheds, correlation between the spatial distributions of streamflow and topographic contributing area decreased during the recession, suggesting a general decrease in the influence of topography on stream base flow contributions. As topographic controls on base flow evidently decreased, multiple aspects of subsurface structure were likely to have gained influence.

1. Introduction

[2]   A primary goal of hydrologic science is to understand the influence of watershed structure on streamflow generation. In watershed-scale studies, the focus has been on relatively large structural elements that tend to change substantially only on the time scale of landscape evolution. Structural elements thought to control spatio-temporal variability in streamflow include both surface characteristics such as topographic contributing area [e.g., *Anderson and Burt*, 1978; *Beven and Kirkby*, 1979; *McGuire et al.*, 2005], and subsurface characteristics such as bedrock structure [e.g., *Huff et al.*, 1982; *Freer et al.*, 2002; *Uchida et al.*, 2008]. Tests of related hypotheses have tended to

focus either on the influence of whole-watershed structure on dynamics at the watershed outlet, or on detailed mechanisms of runoff generation from specific hillslopes. The result is a gap in our understanding of structural controls on streamflow generation between the watershed and hillslope spatial scales. This gap prevents us from locating the sources of water contributing to discharge at a watershed outlet. Thus, closing this gap is important to the most common applications of hydrology, such as: predicting quantity and quality of discharge from ungauged watersheds [e.g., *Sivapalan et al.*, 2003]; characterizing influence of physical hydrologic processes on stream habitat and ecosystem function [e.g., *Stanford and Ward*, 1993; *Montgomery*, 1999]; and locating sources of pollutants within watersheds [e.g., *Kimball et al.*, 2010].

[3]   As noted in commentary from *Beven* [2006], only a few studies have used spatial patterns of stream discharge along valleys to provide direct evidence of structural controls on streamflow generation. These studies suggest that both hillslope topography (e.g., convergence versus divergence [*Anderson and Burt*, 1978]), and bedrock irregularities (e.g., karst conduits [*Huff et al.*, 1982; *Genereux et al.*, 1993]), influence variability in discharge along valleys. The typical extent of these studies has been several hundred meters along a valley, which was sufficient to characterize the influence of the specific hillslope processes

---

[1]Hydrologic Science and Engineering Program, Department of Geology and Geological Engineering, Colorado School of Mines, Golden, Colorado, USA.
[2]Department of Land Resources and Environmental Sciences, Montana State University, Bozeman, Montana, USA.
[3]Department of Civil and Environmental Engineering, Pennsylvania State University, University Park, Pennsylvania, USA.
[4]U. S. Geological Survey, Menlo Park, California, USA.
[5]Pacific Northwest Research Station, United States Department of Agriculture Forest Service, Corvallis, Oregon, USA.

of interest. However, studies limited to these extents cannot reveal the influence of variability in watershed structure beyond the hillslope-scale. Furthermore, only one of these studies [*Genereux et al.*, 1993] examined changes in the spatial distributions of stream discharge when discharge was changing over time. We suggest that more extensive and detailed spatial analyses of streamflow from structurally diverse watersheds will improve understanding of the dominant structural controls on streamflow generation, and repetition of these analyses through time will reveal how the relative influence of these controls may vary with the change in discharge at the watershed outlet [e.g., *Kuraś et al.*, 2008].

[4] The first objective of this study was to identify spatial patterns in stream base flow across a 23 km^2 mountain headwater watershed, and to determine how these patterns were related to the watershed structural elements that were most likely to influence streamflow. Our approach was first to relate spatial variability in stream base flow to topographic contributing area, then to identify potential causes of spatial variability in the resulting discharge-area relationship (i.e., areal yield). The second objective of this study was to determine how the relative influence of various structural elements on stream base flow may change with changes in discharge over time. Our approach was to assess changes in spatial patterns of stream base flow and areal yields during a summer recession in discharge. Spatiotemporal variability in streamflow was characterized using two methods: (1) a more traditional approach using seasonal hydrographs from the study watershed and 5 enclosed subwatersheds (spatially low resolution, temporally high resolution); and (2) detailed spatial distributions of stream base flow along the valleys of the three largest subwatersheds, repeated during 2 to 3 different base flow discharges for each subwatershed (spatially high resolution, temporally low resolution).

[5] Discussion is focused on variability in the relative contributions from subwatersheds and on variability in the relative contributions to valley segments that showed common spatiotemporal trends in base flow generation (segments of ~300 m to 1200 m in length). We describe possible causes of these patterns by comparing relative base flow contributions to spatial distributions of topographic contributing area and other structural elements of the watershed. Finally, we discuss how changes in spatial patterns over the recession suggest a general shift from topographic to subsurface influence on streamflow generation.

2. Study Site

[6] This study was performed at the Tenderfoot Creek Experimental Forest (TCEF), a United States Forest Service research area located in the Little Belt Mountains of central Montana, USA (lat. 46° 55′ N, long. 110° 52′ W). TCEF is drained by Tenderfoot Creek, which is gauged on the main stem downstream of five gauged subwatersheds that are separated by high-relief ridges (Table 1, Figure 1). Here, we refer to the 23 km^2 topographic contributing area to the TCEF outlet gauge as the "TCEF watershed," though the full area of the experimental forest is larger. Tenderfoot Creek flows west to the Smith River, a tributary of the Missouri River.

Table 1. Summary of TCEF Watershed and Subwatershed Characteristics[a]

Name	Gauge Type	Outlet A (km^2)	Elevation Range (m)
TCEF watershed	10 foot Parshall flume[b]	23.0	1986–2426
Stringer	4 foot H flume[b]	5.5	1997–2426
Upper Tenderfoot	4 foot Parshall flume	4.0	2152–2359
Spring Park	2.5 foot Parshall flume	4.5	2104–2426
Sun	4 foot Parshall flume	3.2	2134–2365
Bubbling	3.5 foot H flume	3.6	2040–2361
Lower Tenderfoot area	–	2.2	1986–2243

[a]The Lower Tenderfoot area is the difference between TCEF watershed area and the sum of the five gauged subwatershed areas.

[b]Parshall and H flume stage-discharge relationships developed by the U.S. Department of Agriculture Forest Service [*Brakensiek et al.*, 1979].

### 2.1. Gauged Subwatersheds and Spatial Reference Frame

[7] The five gauged subwatersheds at TCEF are the headwater region of the main stem (Upper Tenderfoot Creek) and the four tributaries that contribute to the main stem between the Upper Tenderfoot Creek gauge and the TCEF watershed outlet gauge (Lower Tenderfoot Creek). These four tributaries are: Stringer Creek in the northwest, Spring Park Creek in the northeast, Sun Creek in the southeast, and Bubbling Creek in the southwest (Figure 1a). The four tributaries are each gauged near their confluence with Lower Tenderfoot Creek (Figure 1b). We refer to the topographic region contributing directly to Lower Tenderfoot Creek, and not the gauged headwaters, as the Lower Tenderfoot contributing area (Figure 1a and 1b).

[8] In addition, stream discharge was studied with approximately 100 m spatial resolution along Stringer, Spring Park, and Upper Tenderfoot Creeks. We refer to locations along each stream by the valley distance upstream of the associated subwatershed gauge (datum of 0 m near each gauge, Figure 2). Valley distance, in contrast to channel distance, does not include the additional length associated with channel sinuosity across the valley floor.

2.2. Summary of Watershed Structure and Vegetation

[9] The TCEF watershed intersects four dominant bedrock units: granite-gneiss, sandstone, shale, and quartz monzonite (Figure 1c) [*Reynolds*, 1995; *Reynolds and Brandt*, 2007]. The northern subwatersheds have greater variability in underlying bedrock than the southern subwatersheds. Intersections of valleys with bedrock contacts create a general convexity in down-valley slopes, such that stream profiles reflect a break from shallower valley slopes in the sandstone regions to steeper valley slopes in granite-gneiss regions (Figures 1b, 1d, and 2).

[10] TCEF uplands are primarily forests of lodgepole pine, *Pinus contorta*, interspersed with a few large meadows, which are commonly referred to as "parks" in maps of the area. Fir (*Abies* spp.) and spruce (*Picea* spp.) are also present and are more common at higher elevations. Nonvegetated patches of talus from the Flathead Sandstone formation are common on the hillslopes of valleys deeply incised into granite-gneiss [*Reynolds*, 1995]. In most locations, plant communities on valley floors (riparian vegetation) are considerably different from upland vegetation,
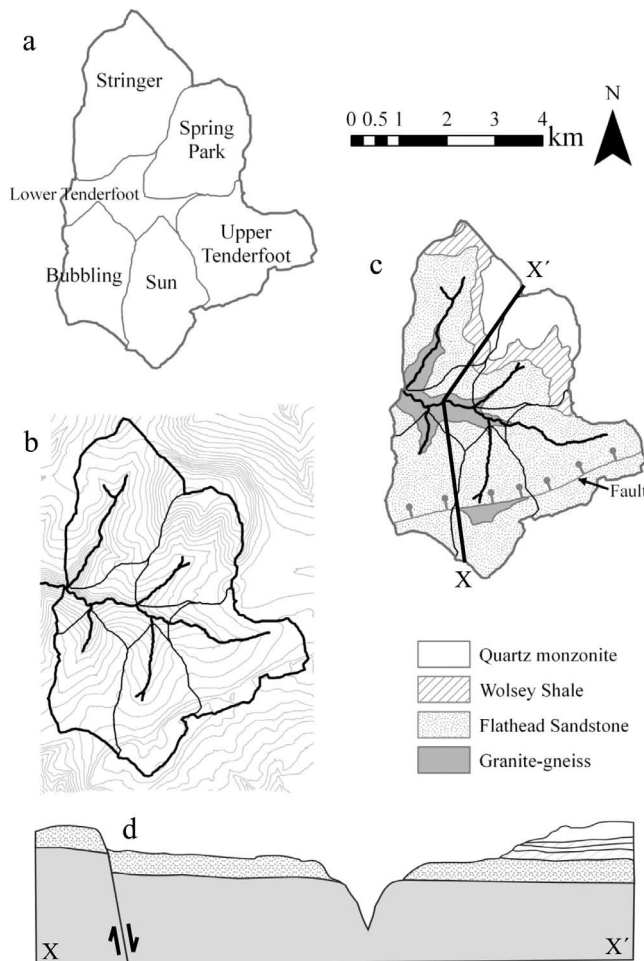
Figure 1. Site map and structural characteristics of the Tenderfoot Creek Experimental Forest watershed (TCEF, lat. 46° 55′ N, long. 110° 52′ W) and its 5 gauged subwatersheds, including (a) names of subwatersheds, (b) topographic map with 20 m contours, (c) underlying bedrock geologic units [*Reynolds and Brandt*, 2007], and (d) an approximate bedrock profile along line X-X′ (enlarged and the vertically exaggerated for clarity) (M. Reynolds, personal communication, 2009). The TCEF outlet gauge and 5 subwatershed gauges are located at the intersection of the stream with its corresponding watershed boundary. The Lower Tenderfoot contributing area is the region of TCEF that does not drain to 1 of the 5 subwatershed gauges.

and vary with valley structure [*Mincemoyer and Birdsall*, 2006].

[11] The sandstone–granite-gneiss contact is located under the Stringer valley floor near 1650 m, resulting in a change in valley slope at this location (from an average of 6% upstream to 9% downstream). However, a substantial change in the Stringer valley hillslope structure is not apparent until a distinct transition just downstream of 1200 m (Figure 2). The segment from 1200 to 0 m in Stringer Creek and much of Lower Tenderfoot Creek have incised deeply into granite-gneiss bedrock and tend to be constrained between high-relief, steep hillslopes (Figures 1c and 2). Riparian vegetation in these valleys is a mosaic of

small meadows interspersed with coniferous trees (spruce, fir, or lodgepole pine). Stream channels in these valleys are tortuous with step-pool sequences created by bedrock outcrops, colluvial materials, and fallen trees.

[12] The segment from 600 to 0 m in Spring Park has incised into granite-gneiss and is somewhat steeper than upstream reaches. However, as with the segment from 1650 to 1200 m in Stringer Creek, this has not yet resulted in a substantial change in the structure of hillslopes. Thus, the valley structure of all of Spring Park Creek and the segment upstream of 1200 m in Stringer Creek are less constrained and have lower-relief hillslopes relative to the valleys deeply incised into granite-gneiss. Valley fill in these segments appear to be more alluvial in nature and have more frequent alluvial channel structures, such as meanders. Vegetation on these valley floors is nearly exclusively meadow, with a distinct boundary between meadow on the valley floor and lodgepole forest on the hillslopes.

[13] Sandstone underlies most of Upper Tenderfoot Creek. However, both valley structure and riparian vegetation change dramatically at around 1400 m (Figure 2). Upstream of this transition, hillslopes have very little relief and riparian vegetation is dominated by a dense spruce-fir forest. Downstream of this transition, hillslope structure and vegetation is comparable to hillslopes of upper Stringer and Spring Park, and riparian vegetation is a mosaic of grassy meadows, scrub willows, and occasional spruce-fir stands.

2.3. Origins of Streamflow and Visible Lateral Contributions

[14] Some of the contributions to stream base flow could be directly observed throughout the summer, particularly at the origins of perennial flow. Flow in the Stringer Creek channel originated from seeps and small springs upstream of 2600 m (Figure 2), and was augmented by a perennial tributary near 2200 m and multiple perennial springs and seeps from 1200 to 900 m. Flow in the Spring Park Creek channel originated from a perennial spring near the contact between the sandstone and overlying shale (∼1400 m, Figure 2) and was augmented by a small perennial tributary just downstream of 1200 m. Flow in the Upper Tenderfoot Creek channel was intermittent upstream of 1400 m and perennial downstream of 1400 m. Upper Tenderfoot Creek was augmented by multiple perennial inflows from relatively short, well-defined channels entering between 1400 and 1100 m. These inflowing channels ultimately originated from seeps and springs in Onion Park, a large meadow located on the south side of a central segment of Upper Tenderfoot Creek (Figure 2).

3. Methods

[15] Data collection and analysis progressed in 3 stages. First, stream discharge was continuously measured at 6 gauges and manually measured with 8 series of dilution-gauging experiments along 3 streams in the watershed. Second, topographic contributing areas were derived from elevation data, and then areal yields (or specific discharge) for the resulting contributing areas were calculated using the discharge data. Third, discharge and areal yield data were normalized to their associated watershed or subwatershed
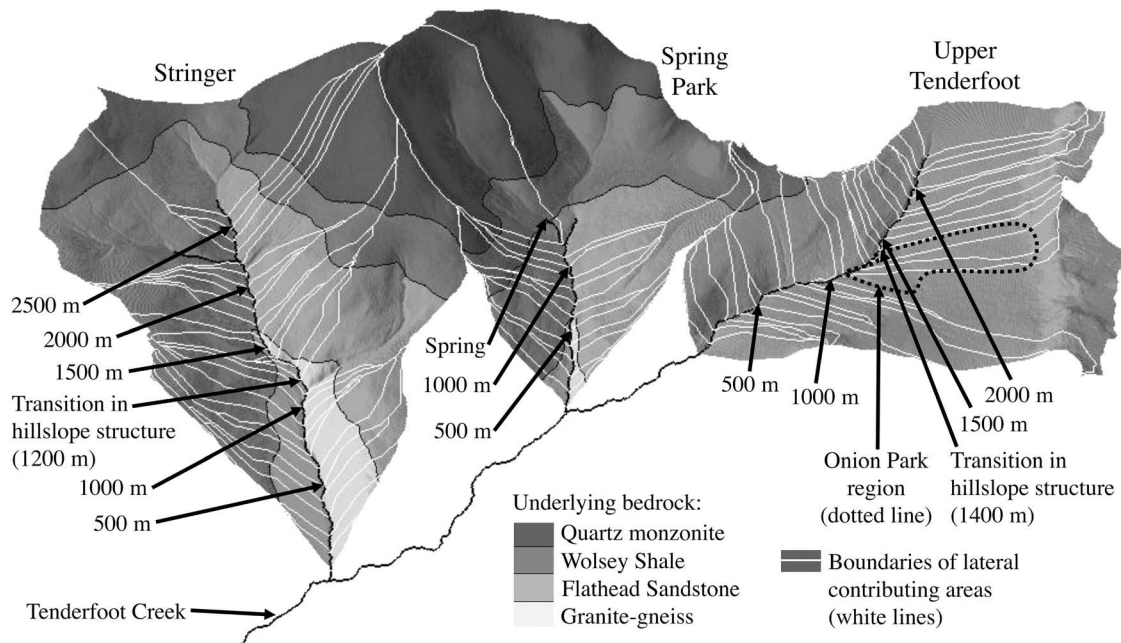
Figure 2. Lateral contributing areas, topographic relief, and underlying bedrock within the three subwatersheds where stream discharge was measured at 100 m intervals along the valley. Topographic relief is rendered in three-dimensional perspective and exaggerated by a factor of 3 to clarify the variability in surface slope. See Figure 1 for orientation and scale information for these subwatersheds because neither a scale bar nor a north arrow can be depicted accurately in this perspective view.

outlet values to facilitate assessment of changes in spatial patterns during the decrease in discharge over the summer.

3.1. Measurement of Stream Discharge and Lateral Inflow

[16] Main stem and subwatershed gauges used for this study were all flumes (Table 1), and stages in attached stilling wells were measured at 15 to 30 min intervals by capacitance rods (TruTrack, New Zealand, note that the use of trade or firm names in this publication is for reader information and does not imply endorsement by the U.S. Department of Agriculture or U.S. Geological Survey of any product or service). Discharges at watershed and subwatershed outlets (Q) were calculated from stage data using rating curves developed by the U.S. Forest Service, and daily average discharges were aggregated from the 15 to 30 min

data. We report 2006 daily average outlet Q from all the headwaters within the TCEF watershed. Flow contributed by the Lower Tenderfoot Area for a given day was calculated as the difference between the TCEF watershed outlet Q and the sum of outlet Q from the five subwatersheds.

[17] Eight longitudinal series of stream discharge measurements were performed in the three largest subwatersheds of the TCEF watershed (Table 1, Figure 1): three series in Stringer Creek, three series in Upper Tenderfoot Creek, and two series in Spring Park Creek. Each series was performed during a different, relatively constant base flow discharge for the respective stream (Table 2). One Upper Tenderfoot Creek series was performed at higher base flow in 2005, and the remaining seven series were performed during the summer base flow recession of 2006. Each series consisted of multiple tracer dilution gauging

Table 2. List of Stream Discharge Dilution-Gauging Series and the Corresponding Discharge Nearest the Subwatershed Outlet From the First Measurement in the Series

Dates	Q(0 m) (L s^{-1})	Q_{SP}(0 m) (mm h^{-1})	Q_{TCEF} (L s^{-1})	$Q_{SP,TCEF}$ (mm h^{-1})
		Stringer		
22–24 Jun 2006	101	0.066	515	0.081
25–28 Jul 2006	21	0.014	151	0.024
26 Aug to 4 Sep 2006	15	0.010	101	0.016
		Upper Tenderfoot		
30 Jun to 1 Jul 2005	89	0.072	722	0.113
29 Jun to 2 Jul 2006	33	0.027	333	0.052
2–3 Aug 2006	14	0.012	129	0.020
		Spring Park		
9–10 Jul 2006	28	0.025	221	0.035
5–6 Aug 2006	14	0.013	122	0.019

measurements along the stream valley. This approach was part of a more detailed assessment of gains and losses in stream channel flow, and the presented flow data from Stringer Creek are derived from the same data set used for a 200 m reach water balance analysis [*Payn et al.*, 2009].

[18] We began each dilution gauging series by measuring discharge near the subwatershed gauge ($Q(0 \text{ m})$). Then, working upstream, we measured Q every 100 m of valley length ($Q(100 \text{ m})$, $Q(200 \text{ m})$, etc., Figure 2a). Series were completed near the origin of measurable channel flow during higher base flow conditions: at 2600 m in Stringer Creek, at 2300 m in Upper Tenderfoot Creek, and at 1200 m in Spring Park Creek. Measurement locations were occasionally moved less than 20 m to avoid locations where the tracer might be poorly mixed with inflows. Locations for discharge measurement were initially selected using measuring tape, then surveyed with an optical total station, and finally recti-fied with high-resolution elevation data from airborne laser swath mapping. The 2005 measurements in Upper Tender-foot Creek were performed according to a slightly different experimental design, such that the data are at less regular intervals and at a somewhat lower spatial resolution than 2006 data. However, 2005 data have sufficient resolution to allow direct comparisons of discharge distributions across a broader range of base flow conditions than 2006 data alone.

[19] Each dilution gauging measurement was made from an independent instantaneous tracer release, such that inac-curacy due to potential tracer mass loss over long transport distances was minimized (see *Payn et al.* [2009] for more details). A known mass of dissolved tracer was released a mixing length upstream of the location of tracer concentra-tion measurement [*Day*, 1977]. Mixing lengths were selected to be long enough for complete mixing, but kept relatively short to minimize tracer mass loss. Mixing lengths included at least three transitions between convergent and divergent channel flow (e.g., pool-riffle sequences) and ranged between 5 and 30 m in valley length, depending on channel structure and flow conditions. We selected dilution gauging over velocity gauging because dilution gauging is likely more accurate in the irregular, tortuous channels of mountain headwaters [*Day*, 1977; *Zellweger et al.*, 1989]. Sodium chloride (NaCl) was used as a conservative tracer, and tracer concentrations were estimated by calibrating temperature-corrected electrical conductivity measurements (EC) to bracketing standard NaCl concentrations made with stream water from the corresponding stream [*Gooseff and McGlynn*, 2005; *Wondzell*, 2006]. EC measurements were made with Campbell CR510 or CR10X data loggers and CS-547A-L temperature/conductivity probes (Campbell Scientific, Inc., Logan, UT, USA). Each probe was independently calibrated in 2006, and a single calibration curve was used for all probes in 2005. All stream EC measurements were corrected for background EC before determining NaCl concentration from the calibration slope.

[20] Dilution of the released tracer mass was used to esti-mate the discharge at a given valley location ($Q(x \text{ m})$) from each concentration breakthrough curve [*Day*, 1977], which assumes steady discharge and complete mass recovery:

$$Q(x\,\text{m}) = \frac{M}{\int\limits_{0}^{t} C(\tau)d\tau}, \qquad (1)$$

where $C(\tau)$ is the tracer concentration breakthrough curve at the base of the reach due to slug mass M, τ is the time variable of integration, and t is the time of EC measurement between the release time ($\tau = 0$) and the return to back-ground EC ($\tau = t$). Breakthrough curves consisted of dis-crete concentration measurements at 2 s intervals, and trapezoidal numerical approximation was used for break-through curve integration. Net lateral inflow per valley dis-tance for a given reach location ($Q_L(x \text{ m})$) was calculated as the net change in flow over the reach (ΔQ) divided by length of the valley (L) along the reach ($Q_L(x \text{ m}) = \Delta Q/L$). "Lateral" is applied in a radial sense, where any surface or subsurface exchange that causes changes between upstream and downstream channel flow is considered lateral. "Inflow" implies the sign convention for the channel water balance, i.e., water contributed to channel flow over a reach is a positive lateral inflow and water lost from the channel over a reach is a negative lateral inflow. In this sense, sour-ces or sinks of lateral inflow may include any combination of surface water, groundwater, or hyporheic flow [*Kuraś et al.*, 2008].

[21] Ideally, longitudinal "snapshots" of discharge measurements would be carried out at exactly the same time. This was impractical for this study, so longitudinal patterns from our sequential method are subject to some bias due to temporal changes in stream discharge [*Kuraś et al.*, 2008]. In this case, discharge tended to decrease over a given series of measurements, due to both diel and sea-sonal patterns. Therefore, individual dilution gauged meas-urements somewhat underestimated the true longitudinal snapshot that corresponded to the time of the first tracer experiment at 0 m. The fraction of underestimation was likely to increase with distance up the valley, due to the cu-mulative time necessary to complete the sequential tracer experiments.

[22] The "worst-case" scenario for temporal bias would coincide with the largest change in discharge during a se-ries of dilution gauging experiments. For example, the maximum temporal bias in a series of experiments in Stringer Creek would have occurred on 22–24 June 2006 (Table 2), when discharge at the outlet gauge ($\sim$0 m) was at its steepest decline (Figure 3) and decreased by 20% dur-ing the 52 h it took to complete the series. To evaluate tem-poral bias in this series, we calculated the fractional temporal change in discharge at the outlet gauge corre-sponding to the time between each upstream dilution gaug-ing measurement (at 100 m, 200 m, etc.) and the dilution gauging measurement nearest the outlet (0 m). Then, each dilution gauged measurement as "corrected" for temporal bias by dividing it by the corresponding fractional temporal change in discharge at the outlet. The result was an average absolute bias of -5 L s^{-1} across the longitudinal series, where the negative value indicates underestimation. This temporal bias is small relative to the 86 L s^{-1} longitudinal change in discharge observed from 2600 m to 0 m, such that the relative patterns of spatial variability were nearly identical between the measured and "corrected" data. We conclude from this worst-case analysis that temporal bias in the data has little influence on our interpretation of spa-tial patterns along our study streams. Furthermore, the tem-poral change in discharge during a few days of experiments is small relative to the change in discharge over the entire
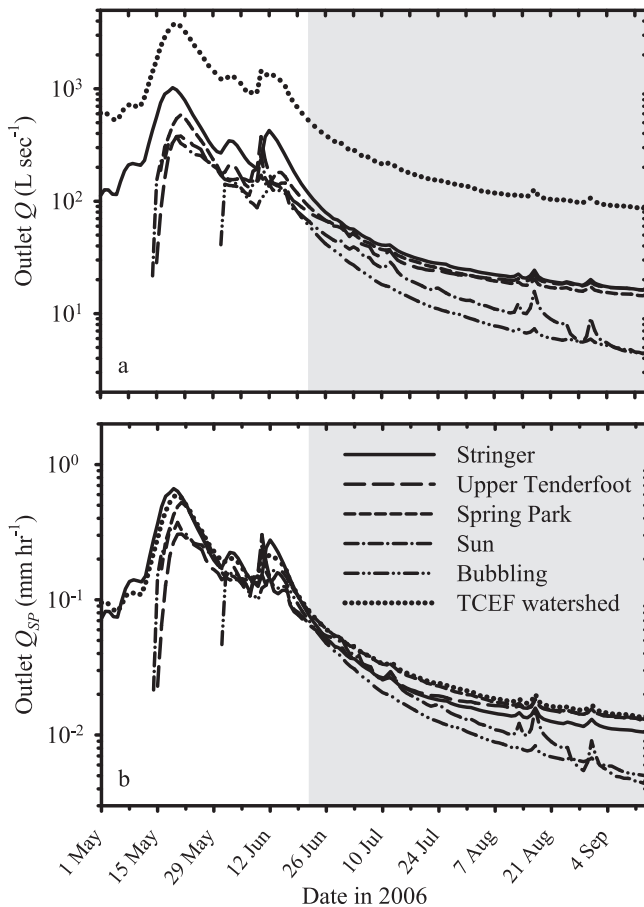
Figure 3. TCEF watershed and subwatershed outlet hydrographs from 2006, including (a) daily mean discharge (outlet Q) and (b) daily mean areal yield (outlet Q_{SP}). The shaded area represents the base flow recession when 2006 dilution gauging series were completed for this study. The threshold effect in the spring is due to thawing in the flumes.

summer, such that temporal biases in individual series have little influence on our analysis of changes in spatial patterns during the recession. Finally, we choose not to report the "corrected" data in this analysis, because the assumptions behind the above estimate of bias are not consistent with our findings. During a given period of time, the fractional temporal change in discharge measured at a subwatershed outlet was not necessarily uniform along the full length of the stream.

3.2. Derivation of Topographic Contributing Area and Areal Yields

[23] Topographic contributing areas were calculated for each location where discharge was measured (Figure 2), including all dilution-gauged (outlet A) and flume-gauged ($A(x$ m)) locations. Topographic analyses were based on digital elevation models (DEM) derived from airborne laser swath mapping. We calculated cumulative contributing area using a multiple-flow-direction analysis of the DEM with 10 m grid cells (MD Infinity, [*Seibert and McGlynn*, 2007]). Multiple-flow-direction algorithms are able to allocate output flow from a single grid cell into multiple adjacent cells, providing a more realistic quantification of

topographic divergence in hillslopes along a stream valley. The Lower Tenderfoot contributing area was calculated by subtracting the sum of subwatershed areas from the total TCEF watershed area (Table 1). We also used a single-flow-direction algorithm [*O'Callaghan and Mark*, 1984] to derive the approximate boundaries of contributing areas for map visualizations (Figures 1 and 2).

[24] We calculated specific discharges at continuous gauges (outlet Q_{SP}) and at locations along stream valleys ($Q_{SP}(x$ m)). In both cases, Q_{SP} was calculated by dividing flow measurements by their respective topographic contributing area ($Q_{SP} = Q/A$ and $Q_{SP}(x$ m) $= Q_{SP}(x$ m)$/A(x$ m)). Lateral contributing areas to stream reaches were calculated from the change in cumulative contributing area (ΔA) over each reach. Lateral specific discharges ($Q_{SPL}(x$ m)) were then calculated from the net change in flow over each reach (ΔQ) divided by its lateral contributing area ($Q_{SPL}(x$ m) $= \Delta Q/\Delta A$). Because this definition of specific discharge is flow normalized to topographic contributing area, we interpret Q_{SP} as topographic "areal yield" and Q_{SPL} as topographic "lateral areal yield" for the purposes of this analysis.

3.3. Normalization of Data to Discharge at the Watershed Outlet

[25] During a seasonal recession uninterrupted by storms, two ubiquitous temporal patterns are expected: (1) flow will decrease at all locations and (2) absolute spatial variability in flow will thus necessarily decrease across all locations. Dominant temporal trends such as these tend to obscure whether contributions to streamflow from a given location have an increasing or decreasing influence on discharge at the watershed outlet through time. Thus, normalization to discharge at the outlet provides a straightforward spatial reference frame for direct interpretation of dynamics in these relative contributions. However, as with all normalization schemes, care should be taken that inferences made from increasing relative contributions are not artificially extended to the ubiquitously decreasing absolute trends.

[26] Distributed stream discharge data were normalized to the corresponding watershed or subwatershed outlet discharge data. Daily average Q and Q_{SP} from the subwatershed gauges and Lower Tenderfoot areas were normalized to the daily average Q for the same day from the TCEF watershed gauge (Q_{TCEF} and $Q_{SP, TCEF}$). Each resulting relative discharge ($Q^* = Q/Q_{TCEF}$, Table 3) represents the fraction discharge at the TCEF outlet that was attributable to the corresponding subwatershed outlet or the Lower Tenderfoot contributing area. Therefore, the sum of all Q^* must be 1.0 for a given day, because the contribution from the Lower Tenderfoot area was determined by difference. The relative areal yields ($Q_{SP}^* = Q_{SP}/Q_{SP, TCEF}$, Table 3) represent the fraction of TCEF areal yield associated with the corresponding subwatershed outlet or the Lower Tenderfoot contributing area. Values of $Q_{SP}^* > 1.0$ indicate areas with disproportionately larger yields than the overall TCEF watershed, and values of $Q_{SP}^* < 1.0$ indicate areas with disproportionately smaller yields.

[27] Similarly, $Q(x$ m) and $Q_{SP}(x$ m) measured by dilution gauging along streams (at x m along a valley) were normalized to the $Q(0$ m) and $Q_{SP}(0$ m) from the dilution-gauged discharge measurement nearest the subwatershed outlet from

Table 3. Summary of Variables Used to Describe Contributing Area, Stream Discharge, Lateral Contributions to Stream Discharge, and Their Relationships[a]

		Stream Channel Flow		Lateral Contributions	
Type of Measure	Contributing Area	Discharge	Specific Discharge (or Areal Yield)	Net Inflow	Specific Discharge (or Areal Yield)
Absolute	A [L^2]	Q [L^3 T^{-1}]	Q_{SP} [L T^{-1}]	Q_L [L^3 T^{-1} L^{-1}]	Q_{SPL} [L T^{-1}]
Relative to outlet[b]	A^* [-]	Q^* [-]	Q_{SP}^* [-]	Q_L^* [L^{-1}]	Q_{SPL}^* [-]

[a]Variable dimensions (L = length, T = time) are provided beside each variable.
[b]Relative to the TCEF outlet in the case of flume gauged measurements at subwatershed outlets (Q^*, Q_{SP}^*) and relative to the subwatershed outlet in the case of dilution gauged measurements along stream valleys (Q^* (x m), Q_{SP}^* (x m), Q_L^* (x m), and Q_{SPL}^*(x m)).

the same measurement series ($Q^*(x$ m$) = Q(x$ m$)/Q(0$ m$)$ and $Q_{SP}^*(x$ m$) = Q_{SP}(x$ m$)/Q_{SP}(0$ m$)$, Table 3). $Q_L(x$ m$)$ and $Q_{SPL}(x$ m$)$ were also normalized to the associated $Q(0$ m$)$ and $Q_{SP}(0$ m$)$, to quantify the relative lateral contribution to flow ($Q_L^*(x$ m$) = Q_L(x$ m$)/Q(0$ m$)$) and relative lateral areal yield ($Q_{SPL}^*(x$ m$) = Q_{SPL}(x$ m$)/Q_{SP}(0$ m$)$, Table 3) for stream reaches. In this case, $Q_L^*(x$ m$)$ is the fraction of outlet discharge gained (+, net gaining reach) or lost (−, net losing reach) per 100 m of valley length, and $Q_{SPL}^*(x$ m$)$ is the fraction of the subwatershed areal yield associated with a given lateral contributing area. As with Q_{SP}^* for subwatersheds, values of $Q_{SPL}^*(x$ m$) > 1.0$ indicate lateral areas with disproportionally larger yields than the corresponding subwatershed, and values of $Q_{SPL}^*(x$ m$) < 1.0$ indicate lateral areas with disproportionally smaller yields.

[28] Finally, $A(x$ m$)$ at each dilution gauged location was similarly normalized to the $A(0$ m$)$ of the corresponding subwatershed ($A^*(x$ m$) = A(x$ m$)/A(0$ m$)$, Table 1, Figure 2). The resulting topographic area accumulation curves ($A^*(x$ m$)$ versus x) can be compared directly with longitudinal $Q^*(x$ m$)$ distributions on the same scale. In this comparison, correlation of $Q^*(x$ m$)$ with $A^*(x$ m$)$ would suggest a linear topographic control of streamflow generation, and the local slope of $Q^*(x$ m$)$ versus $A^*(x$ m$)$ is equal to $Q_{SPL}^*(x$ m$)$. We quantified the fraction of variability in stream discharge linearly described by accumulated contributing area by calculating the coefficient of determination (R^2) of $Q^*(x$ m$)$ versus $A^*(x$ m$)$ along valleys. $Q^*(x$ m$)$ and $A^*(x$ m$)$ along the same valley are inherently cumulative and nonindependent data, so the R^2 statistic is always relatively near 1 in generally gaining streams. Therefore, this statistic is used only for description of relative changes in the relationship and not for direct inference.

4. Results

[29] Most of the 2006 annual runoff at TCEF was driven by snowmelt and spring storms (Figure 3). Summer storms in 2006 had negligible influence on stream discharge relative to annual runoff, resulting in a generally smooth summer recession. Summer recession rates of outlet Q and Q_{SP} varied among the subwatersheds, particularly when comparing the southern subwatersheds (Sun and Bubbling) with the rest of the TCEF watershed. The Sun and Bubbling subwatersheds had similar outlet Q_{SP} to other subwatersheds early in the recession, but the lowest outlet Q and Q_{SP} by the end of the summer recession (Figure 3). Spring Park and Upper Tenderfoot subwatersheds had the smallest absolute changes in outlet Q over the recession (Figure 3a), demonstrating more consistent sources of runoff through the summer. The Stringer subwatershed contributed more

water than any other subwatershed during peak flows and early recession, but receded to similar flows as Spring Park and Upper Tenderfoot by the end of the summer. Variability in subwatershed outlet Q_{SP} ranged from 0.07 to 0.1 mm h^{-1} at the beginning of the study period and from 0.004 to 0.013 mm h^{-1} at the end of the study period (Figure 3b).

4.1. Relative Contributions From TCEF Subwatersheds and Lower Tenderfoot

[30] Relative flow contributions and areal yields from the five headwater subwatersheds showed three general trends with decreasing discharge at the TCEF outlet (Figure 4). The first trend was a rapid decline of relative contribution
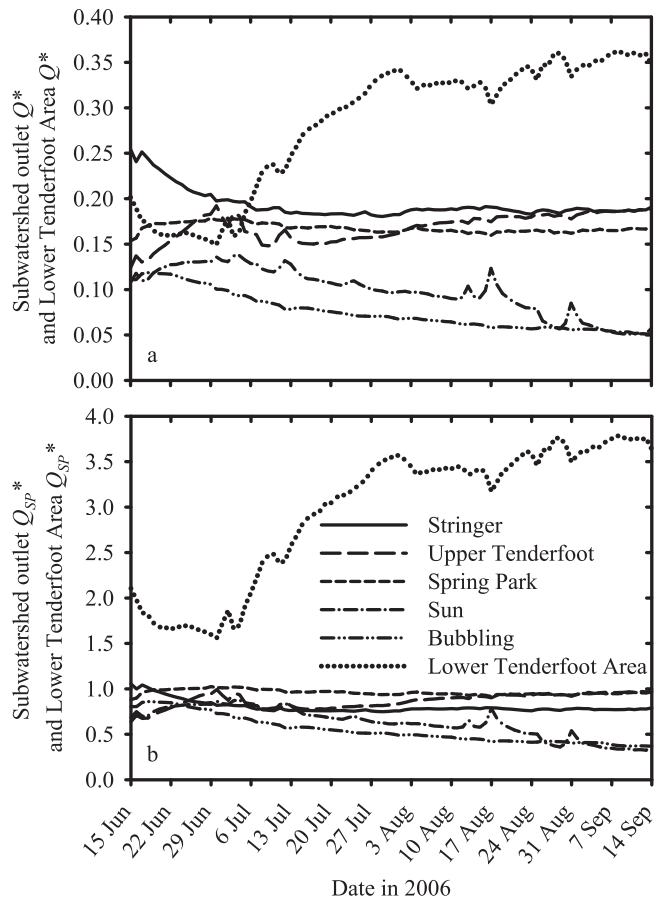
Figure 4. (a) Relative contributions to 2006 TCEF outlet base flow (Q^*) and (b) corresponding relative areal yields (Q_{SP}) from the subwatershed outlets and the Lower Tenderfoot contributing area.

early in the recession, followed by a relatively high and constant contribution through the remainder of the summer. For example, outlet Q^* from Stringer decreased from ~0.25 to 0.18 during the first three weeks of the recession, and subsequently remained near 0.18 through the rest of the summer (Figure 4a). Stringer was the largest contributor among the subwatersheds (excluding the Lower Tenderfoot area), but its relative areal yield (or outlet Q_{SP}^*) was ~20% lower than that of Upper Tenderfoot and Spring Park during the latter half of the recession (Figure 4b). The second trend was a relative flow contribution that remained nearly constant or increased slowly during most of the recession. For example, outlet Q^* from Spring Park ranged between ~0.15 and 0.18 through the entire recession (Figure 4a). Outlet Q^* from Upper Tenderfoot ranged between ~0.12 and 0.19, exhibiting more variability early in the recession and slowly increasing through the remainder of the summer. The relative yields at the outlets of both these subwatersheds were comparable to TCEF outlet yields by the end of the summer (outlet $Q_{SP}^* \approx 1$), but relative yields at the Upper Tenderfoot outlet were somewhat lower earlier in the summer (Figure 4b). The third trend was a general decrease in relative contribution during the entire recession. For example, outlet Q^* from Sun and Bubbling steadily decreased from ~0.14 to 0.05 during the majority of the recession, with the exception of relatively flashy storm responses in Sun Creek. Areal yields at the Sun and Bubbling outlets were similar to those of other headwater subwatersheds early in the summer (Figure 4b), despite their lower relative contributions to TCEF outlet flow.

[31] The Q^* from the Lower Tenderfoot area quickly increased to the largest relative contribution in early July, as the relative contribution from the subwatersheds decreased (Figure 4a). At the end of the summer recession, the Lower Tenderfoot area contributed nearly 2 times the flow of the subwatershed with the highest outlet Q^* (either Spring Park or Upper Tenderfoot), or approximately 35% of the discharge at the TCEF watershed outlet. This large relative contribution corresponded with a disproportionately high areal yield, over 3.5 times that of the TCEF watershed as a whole (Figure 4b).

4.2. Distribution of Discharge, Contributing Area, and Yield Along Streams

[32] Series of discharge measurements along streams reflect multiple base flow discharges during the recession (Table 2), where discharge measured nearest the outlet ($Q(0 \text{ m})$) ranged over nearly an order of magnitude in Stringer Creek (15, 21, and 101 L s^{-1}, Figure 5a) and Upper Tenderfoot Creek (14, 33, and 89 L s^{-1}, Figure 5b). Higher baseflows were not sampled in Spring Park Creek, so $Q(0 \text{ m})$ differed by only two-fold between the two series of measurements (14 and 28 L s^{-1}, Figure 5c).

[33] Longitudinal distributions of $Q(x \text{ m})$ show that valley segments from 300 to 1200 m in length had similar trends in net change in discharge along each valley (Figure 5). For the purposes of this paper, we refer to this as "segment-scale" variability (300 to 1200 m) to differentiate from the "reach-scale" resolution of the data (~100 m). In many cases, abrupt transitions between adjacent segments had a distinct location (within 100 m) where the lateral contributions to streamflow sharply increased (e.g., 1400 m in Upper Tenderfoot Creek and 1200 m in Stringer Creek) or decreased (e.g., 1100 m in Upper Tenderfoot Creek) with distance downvalley (Figure 6). These transitions resulted in sharp inflections in the relative accumulation of streamflow along the valley ($Q^*(x \text{ m})$). Locations of these transitions were consistent through multiple base flow discharge conditions, and variability in relative flow contributions among these segments tended to increase during the recession.
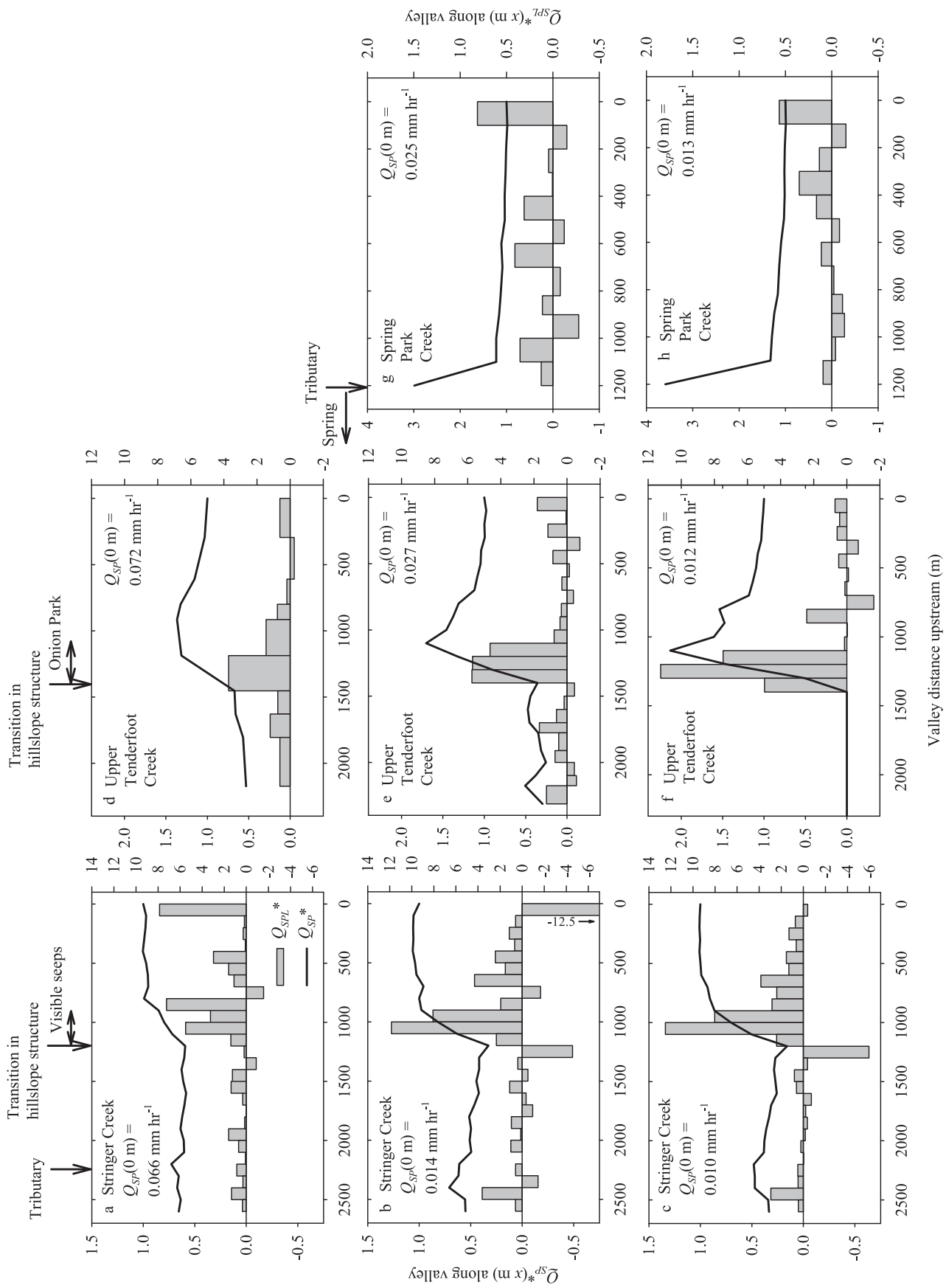
[34] Changes in the discrete relative contributions of 100 m reaches emphasize the increase in relative variability among valley segments, as quantified by $Q_L^*(x \text{ m})$ (Figure 6) and $Q_{SPL}^*(x \text{ m})$ (Figure 7) of reaches within each segment. The high spatial resolution of these flow data allows more precise delineation of the transitions between the valley segments. However, these high-resolution data also reveal the potential for reach-scale variability in stream base flow generation (i.e., variability among individual 100 m reaches within a segment). Some of this variability may have been introduced by compounded errors from the multiple flow measurements necessary to estimate net change in discharge over a reach [*Kuraś et al.* 2008]. However, detailed analyses
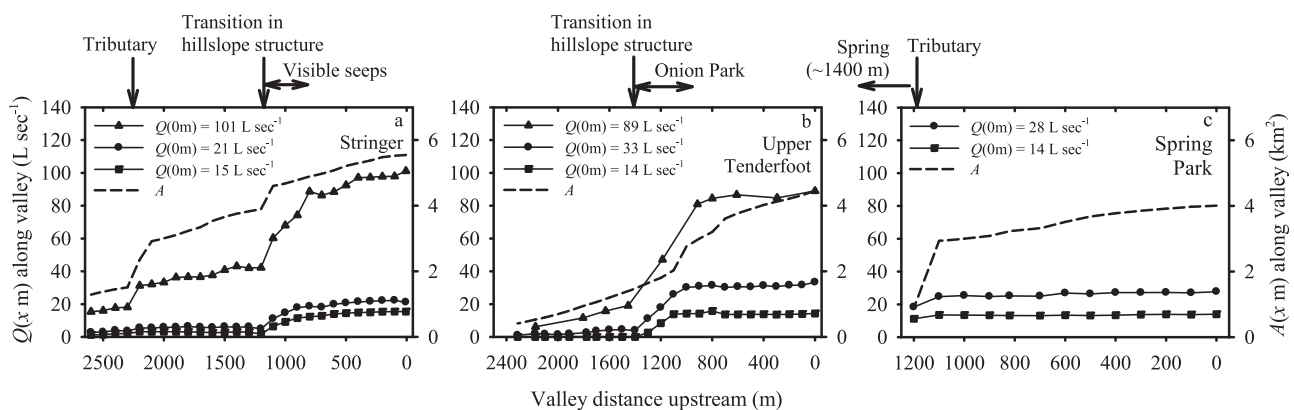
Figure 5. Longitudinal distributions of stream discharge ($Q(x \text{ m})$) and topographic contributing area ($A(x \text{ m})$) along the valleys of (a) Stringer Creek, (b) Upper Tenderfoot Creek, and (c) Spring Park Creek. Locations of some notable hydrologic and structural features from Figure 2 are cross-referenced above the graphs.

Figure 6. Longitudinal distributions of local discharge relative to outlet discharge ($Q^*(x m)$, solid lines), accumulated contributing area relative to outlet contributing area ($A^*(x m)$ dashed lines), and lateral streamflow contributions relative to outlet discharge ($\tilde{Q}_L^*(x m)$, bars) along the valleys of (a–c) Stringer Creek, (d–f) Upper Tenderfoot Creek, and (g and h) Spring Park Creek. Figures for each stream are stacked in order of decreasing flow at the outlet. Locations of some notable hydrologic and structural features from Figure 2 are cross-referenced above the graphs.

Figure 7. Longitudinal distributions of local areal yield relative to outlet areal yield ($Q_{SP}^*(x\ m)$, lines) and lateral areal yield ($Q_{SPL}^*(x\ m)$, bars) along the valleys of (a–c) Stringer Creek, (d–f) Upper Tenderfoot Creek, and (g and h) Spring Park Creek. Figures for each stream are stacked in order of decreasing flow at the outlet. Locations of notable hydrologic and structural features from Figure 2 are cross-referenced above the graphs.

of the causes of reach-scale variability are outside the scope of this study, and will ultimately require a hierarchical model that first accounts for the larger segment-scale variability. Therefore, we focus our interpretations on more general trends that appear to dominate among segments, and these interpretations do not rely on subtle patterns or small differences among individual reaches.

[35] Variability in net lateral inflow along Stringer Creek demonstrated generally lower yields upstream and higher yields downstream, which we organized into 4 valley segments with distinct trends in $Q(x$ m$)$ and $Q^*(x$ m$)$ over space and time (Figures 5a and 6a–6c). (1) A moderately gaining valley segment from 2600 to 2200 m was located near the initiation of flow. This segment included substantial gains from the small tributary (over the 2300 to 2200 m reach), which showed yields similar to the other contributing areas in this segment (Figure 7a–7c). However, $Q_{SP}^*(2200$ m$)$ shows that yield at the downstream end of this segment was only 50–65% of the watershed yield at any time during the recession. (2) The valley segment from 2200 to 1200 m crossed the bedrock contact and changed from marginally net gaining to marginally net losing during the recession. This segment only contributed substantial base flow early in the recession. (3) The valley segment from 1200 to 900 m is located just downstream of the transition in hillslope structure and was strongly gaining in all longitudinal series of discharge measurements. $Q_{SPL}^*(x$ m$)$ for reaches in this segment indicate contributing areas with a disproportionately large influence on the Stringer subwatershed yield, and this relative influence on yield increased during the recession. (4) The valley segment from 900 to 0 m was moderately net gaining in all longitudinal series of discharge measurements.

[36] A centrally located valley segment along Upper Tenderfoot Creek contributed most of the discharge from the subwatershed, splitting the stream into 3 segments with distinct trends in base flow over space and time (Figures 5b and 6d–6f). (1) The valley segment from 2300 to 1400 m was intermittent, with moderate gains when surface flow was present. (2) The valley segment from 1400 to 1100 m was located just downstream of the change in valley structure from lower to higher relief hillslopes, and ran adjacent to Onion Park. This segment was the dominant source of outlet discharge through the recession, consistently resulting in a peak $Q_{SP}^*(1100$ m$)$ greater than 1 at the downstream end of this segment (Figure 7d–7f). (3) The valley segment from 1100 to 0 m was marginally net gaining to net neutral, and did not appear to be a substantial source of outlet discharge at any time in the recession.

[37] Patterns of lateral inflow along Spring Park Creek were quite different from those of Stringer Creek or Upper Tenderfoot Creek, due to the substantial fraction of subwatershed base flow originating at the spring upstream of 1200 m (Figures 5c and 6g–6h). $Q^*(1200$ m$)$ nearest the spring showed that channel flow was already 60% of outlet base flow earlier in the recession and increased to 80% of outlet baseflows later in the recession. The $Q_{SP}^*(1200$ m$)$ nearest the spring was much larger than 1 during both measurement periods, showing that the topographic contributing area to the spring had a disproportionately large contribution to outlet discharge relative to the rest of the Spring Park subwatershed (Figures 7g and 7h). Immediately

downstream, $Q_{SP}^*(1100$ m$)$ indicated a sharp decrease in yield along the reach from 1200 to 1100 m, due to a large increase in contributing area relative to the discharge in the tributary contributing to this reach (Figures 7g and 7h). The remaining valley segment from 1100 to 0 m crossed the bedrock contact, and contributed little to discharge at the subwatershed outlet throughout the base flow recession.

[38] With decrease in discharge, topographic contributing area linearly explained less spatial variability in stream base flow in all three streams studied in detail. This is quantified by a decrease in the R^2 statistic of the $Q^*(x$ m$)$ versus $A^*(x$ m$)$ relationship with decrease in base flow in each of the streams (Figure 6). The decrease in the coefficient of determination was necessarily coincident with the general increase in the longitudinal variability of $Q_{SP}^*(x$ m$)$ and $Q_{SPL}^*(x$ m$)$ observed in each stream. The only exception to this pattern was the $Q_{SPL}^*(x$ m$)$ in Spring Park Creek (Figure 7), where the downstream lateral yields were all low relative to the yield nearest the spring.

5. Discussion

[39] Contributions to stream base flow were spatially variable at the subwatershed scale (Figure 4a) as well as at the 300 to 1200 m segment scale along each headwater stream studied in detail (Figures 5 and 6). Streamflow generally increased with distance down valleys, thus cumulative streamflow was necessarily positively correlated with cumulative topographic contributing area (Figure 6). However, the relationship between streamflow and contributing area varied across the watershed and along streams (Figures 4b, 6, and 7). This indicates spatial variability in base flow contribution that is not attributable to topographic contributing area alone, particularly late in the recession. Under base flow conditions, the next most likely explanations for variability in streamflow are associated with subsurface structure.

5.1. Potential Subsurface Influences on Base Flow

[40] In sections 5.1.1 to 5.1.3, we present a few common hydrologic hypotheses that may explain how spatial variability in streamflow and areal yield across TCEF may be related to components of subsurface watershed structure. Our purpose is not to rigorously support or disprove individual hypotheses. We recognize the presented data are insufficient for this task. Our purpose is to put TCEF base flow data in the context of streamflow generation mechanisms supported by current literature, with an emphasis on the potential for multiple mechanisms to overlap in a given region of the watershed. Through this exercise, we provide a more mechanistic and spatially explicit hydrologic exploration than the typical analysis of time series at watershed outlets, alone.

5.1.1. Influence of Bedrock Transitions on Storage and Flow Direction
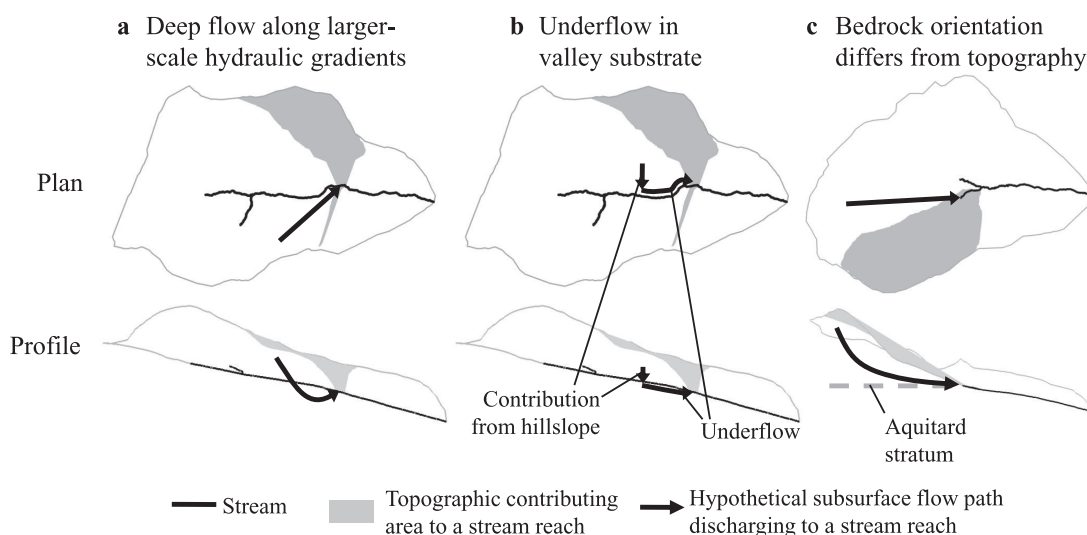
[41] Variability in streamflow and areal yields between sandstone and granite-gneiss regions (Figures 1c and 2) suggest that underlying bedrock and its daughter materials are likely to influence contributions to streamflow. Deeper incision into granite-gneiss may explain the large contributions from the Lower Tenderfoot area relative to the subwatersheds, particularly later in the recession (Figure 4). Also, within the Stringer subwatershed, the segment deeply incised

into granite-gneiss bedrock (1200 to 0 m) consistently contributed more to subwatershed outlet flow than upstream segments (2600 to 1200 m, Figures 6a–6c and 7a–7c).

[42] Variability in streamflow generation associated with the sandstone–granite-gneiss interface may be explained by differences in subsurface storage characteristics among the lateral contributing areas. Valleys deeply incised into granite-gneiss have high-relief hillslopes, and these hillslopes are underlain by substantial areas of both granite-gneiss at lower elevations and sandstone at higher elevations (Figures 1 and 2). Hence, these valley segments may have received contributions from deep storage under adjacent hillslopes [*Uchida et al.*, 2008] or may have received contributions from bedrock, weathered materials, and/or soils with a higher storage capacity within their respective topographic contributing areas [*Harman et al.*, 2009; *Jencso and McGlynn*, 2011]. Also, the length, slope, or other characteristics of shallow flowpath orientation in the contributing area may influence their storage capacity [*McGlynn et al.*, 2003; *McGuire et al.*, 2005]. All of these mechanisms may be summarized in the context of topographic recharge areas that have varying rates of recession, where "fast" draining areas are dominant contributors early in the recession and "slow" draining areas are dominant contributors later in the recession.

[43] Variability in streamflow generation may also arise from subsurface contributing areas that differ from topographic contributing areas. To distinguish between "subsurface" and "topographic" contributing areas, we define "subsurface contributing area" as the recharge region delineated by the full collection of subsurface flow paths that ultimately discharge to a given location on a stream. By this definition, the subsurface contributing area to a given location may not agree with the corresponding topographic contributing area derived from surface flow direction alone. For example, in the topographically driven flow networks proposed by *Tóth* [1963], shallower flow paths induced by smaller-scale topographic variability are nested within deeper flow paths induced by larger-scale topographic variability. At TCEF, valleys deeply incised into granite-gneiss may intersect larger-scale subsurface flow paths and/or preferential flow paths that are recharged beyond the boundaries of topographic contributing areas (in the sense of *Wörman et al.* [2007] and *Gleeson and Manning* [2008]). More specifically, larger-scale, deeper flow paths in the Stringer subwatershed may have moved water from recharge at upper elevations to discharge in the stream at lower elevations, if flow through sandstone bedrock was possible (Figure 8a). This may explain the visible springs and seeps present along the hillslopes from 900 m to 1200 m, near the sandstone–granite-gneiss contact. Hydrologic characteristics of the Flathead Sandstone suggest that deep flow paths would be limited to fractures, rather than pores [*Reynolds*, 1995]. Where flow paths such as these are a dominant source of streamflow, subsurface contributing areas are not likely to agree with topographic contributing areas derived from a 10 m resolution topographic analysis. Contributions from large scale flow paths may also explain the increase in the relative contribution from the Lower Tenderfoot contributing area during the recession (Figure 4a), and may explain why that contribution was strongly disproportionate to its relatively small contributing area (Figure 4b). Finally, fracture flow at the sandstone–granite-gneiss contact may have promoted development of preferential flow paths on top of the granite-gneiss unit [*Hewlett*, 1969; *Genereux et al.*, 1993; *Freer et al.*, 2002], resulting in disagreement

a Deep flow along larger-scale hydraulic gradients   **b** Underflow in valley substrate   **c** Bedrock orientation differs from topography

Plan

Profile

Contribution from hillslope   Underflow   Aquitard stratum

—— Stream   [gray] Topographic contributing area to a stream reach   → Hypothetical subsurface flow path discharging to a stream reach

Figure 8. Hypothetical groundwater flow paths to a stream reach (arrows) that are feasibly recharged by regions outside the topographic contributing area to that reach (gray regions). Paired plan and profile views of subwatersheds and reaches from the current study are used for illustration, and elevations are exaggerated 3X to clarify changes in slope. Example flow paths are: (a) 1100–1200 m in Stringer Creek: larger-scale hydraulic gradients may create long flow paths that recharge in uplands and provide gains to streamflow in downstream reaches; (b) 1100–1200 m in Stringer Creek: shallow underflow in the valley floor may connect downstream stream channel gains to upstream hillslopes; (c) upstream of 1200 m in Spring Park Creek: orientation of bedrock contacts may create a perched aquifer and change the direction of subsurface flow relative to gradients suggested by surface topography.

between the flow directions suggested by the land surface and the granite-gneiss surface.

5.1.2. Influence of Transitions in Valley Floor Structure

[44] The sandstone–granite-gneiss interface may indirectly influence the location of streamflow contributions through its influence on valley floor structure. Where underflow is substantial along a stream segment, upstream contributions from hillslopes may flow in the shallow valley subsurface for long distances before being forced into the downstream surface channel [*Larkin and Sharp*, 1992]. Contributing areas to these segments would thus have lower apparent yields to channel flow, even if the contributions from hillslopes were similar to other areas of the watershed. This may partially explain the tendency for sandstone dominated valleys of TCEF with more alluvial sediment to exhibit lower lateral areal yields (e.g., upper reaches of Stringer Creek, Spring Park Creek, and most of Upper Tenderfoot Creek). In particular, this may explain the flow patterns observed near 1200 m in Stringer Creek. Just downstream of 1200 m, valley floor alluvium is "pinched" at the transition to the more constrained valley, which is likely to force underflow in upstream alluvium into the channel [*Stanford and Ward*, 1993; *Baxter and Hauer*, 2000]. Therefore, at least some of the relatively large contribution observed in the 1200 to 1100 m reach of Stringer Creek (Figures 6a–6c) may have been connected to sources in hillslopes upstream of 1200 m through relatively shallow subsurface flow paths in the valley floor (Figure 8b).

[45] We examined the potential influence of subsurface down-valley flow in Stringer Creek through simplified alternative estimates of underflow immediately upstream of 1200 m. First, we assumed that all down-valley flow in sediment upstream of 1200 m was forced to the surface immediately downstream of 1200 m. Then, we assumed uniform, isotropic Darcian flow along a 6% gradient and across a 13 m^2 cross-sectional area, based on a valley width of 13 m and a saturated sediment depth of 1 m [*Jencso et al.*, 2009]. If uniform hydraulic conductivity of valley-floor sediment was 10^{-4} m s^{-1} (considered typical for highly conductive river beds [*Larkin and Sharp*, 1992]), underflow discharge downstream of 1200 m would have been 0.08 L s^{-1}, which explains a negligible portion of the 5 L s^{-1} net gain from 1200 m to 1100 m during the lowest discharge conditions ($Q(0\ m) = 15$ L s^{-1}, Figure 5a). Alternatively, uniform hydraulic conductivity would need to have been 3×10^{-3} m s^{-1} for underflow to explain half the net gain from 1200 to 1100 m at this time (2.5 L s^{-1}). This estimate of conductivity would be expected in clean sand or gravel [*Freeze and Cherry*, 1979]. A uniform composition of clean sand or gravel is unlikely at this location in Stringer Creek, but this estimate of conductivity may be reasonable if some portion of the 13 m^2 cross-sectional area included highly conductive preferential flow paths (e.g., relict channels [*Poole et al.*, 2002]). In either case, it is likely that a substantial amount of the net gain in the reach from 1200 to 1100 m was provided by sources other than underflow forced to the surface, and these alternative sources of flow were evident in the springs and seeps emerging from the hillslopes along this reach (see section 5.1.1. and Figure 8a).

5.1.3. Contributions to Base Flow From Upstream Regions

[46] Upstream regions of the Spring Park and Upper Tenderfoot subwatersheds contributed substantial amounts of TCEF outlet flow, especially later in the summer. At the lowest discharge, the combined flow from Spring Park and Upper Tenderfoot subwatersheds contributed 36% of discharge at the TCEF outlet, and each contributed nearly the same fraction as Stringer Creek (Figure 4a). Upstream regions within the Spring Park and Upper Tenderfoot subwatersheds provided the majority of the streamflow at their gauges, where downstream regions closest to the gauges (>1 km of valley length) showed little to no lateral contribution to streamflow (Figures 6d–6h).

[47] One explanation for the relatively strong contribution from the spring at the origin of Spring Park Creek is a perched aquifer on an aquitard [*Reynolds*, 1995]. The spring emerges near the contact of the sandstone and shale formations. Above the contact, alternating beds of shale and intrusive monzonite are overlain by a thick layer of monzonite composing the ridge on the north side of the watershed (Figures 1c and 1d). The orientation of these strata (Figure 1d) may create a perched aquifer that is recharged by a subsurface contributing area much larger than the topographic contributing area, especially in the generally divergent landscape near the spring (Figure 8c). Regardless of the mechanism, the co-occurrence of a relatively large contribution from the spring (Figures 6g–6h) and the consistency of the relative contribution of the Spring Park subwatershed (Figure 4a) suggest extensive storage in the ridge, which is likely influenced by the bedrock strata underlying the northern ridge of the watershed (Figures 1c and 1d).

[48] Base flow contributions from the Upper Tenderfoot subwatershed were concentrated along the stream from 1400 to 1100 m. These contributions originated primarily from Onion Park, a large meadow located immediately south of this segment (Figure 2). There is no known bedrock feature to explain the location of these substantial gains in streamflow; though like Spring Park, the relatively consistent contribution from the Upper Tenderfoot subwatershed (Figure 4a) suggests the presence of more extensive storage in contributing areas to the upstream regions of TCEF. The shape of the lateral topographic contributing area suggests the potential for relatively long and low-gradient flow paths near the surface in this region (Figure 2), perhaps explaining increased potential for hydrologic storage [*McGuire et al.*, 2005].

5.2. Seasonal Change in the Base Flow: Area Relationship

[49] Regardless of the specific hydrologic mechanisms of flow generation that were active within the TCEF watershed, spatio-temporal distributions of base flow reflected an apparent decay in direct topographic control on streamflow generation. This trend was most evident in the ubiquitous increase in spatial variability of relative areal yields through the recession, both across and within subwatersheds. While topographic control decreased, the controls that gained influence may be explained by multiple components of subsurface structure, as suggested above. Higher correlations between streamflow and contributing area

during higher baseflows at TCEF may be related to stronger influence of topographic contributing during the snow melt season, when there are more shallow flow paths that are hydrologically connected to the stream [*Jencso et al.*, 2009, 2010]. Even so, *Jencso et al.* [2011] as well as *Kuraś et al.* [2008] suggest that variables other than topographic contributing area are necessary to predict the spatial distribution of higher flows caused by storm and snowmelt response. In general, we suggest that the observed changes in spatial patterns of relative yield through the recession reflect a gradual transition from topographic to subsurface controls on the contributions to stream base flow.

5.3. Comparisons With Similar Studies and Implications for Future Studies

[50] Further hydrologic insights about both hillslopes and watersheds can be gained from more comparisons of valley structure with longitudinal streamflow variability [*Beven*, 2006]. The present study joins a few others that have directly assessed changes in streamflow along valleys at high resolution to show that accumulated area generally controls accumulated streamflow [*Anderson and Burt*, 1978; *Huff et al.*, 1982], but other mechanisms related to subsurface structure are also important in certain geologic contexts or flow conditions [*Huff et al.*, 1982; *Genereux et al.*, 1993]. Furthermore, similar to *Genereux et al.* [1993], we demonstrate an apparent shift in the dominant controls of streamflow generation with changing discharge conditions. These earlier studies only examined stream reaches approximately 300 to 550 m in length [*Anderson and Burt*, 1978; *Huff et al.*, 1982, *Genereux et al.*, 1993], and two of these studies were conducted in the same stream segment [*Huff et al.*, 1982; *Genereux et al.*, 1993]. In contrast, the current study examined the spatial distribution of streamflow generation over a larger area, and was able to reveal segment-scale spatial variability in streamflow that would not have been discernible in the previous work. The existence of segment-scale variability is not surprising, but has not been extensively described with field data. Furthermore, it falls between the watershed-scale and hillslope-scale of variability that are more typically addressed in designs of hydrologic field studies.

[51] *Kuraś et al.* [2008] performed a similarly extensive study of lateral inflows in all the streams of a smaller watershed (4.7 km^2) at a somewhat coarser resolution (~200 to 500 m). They also found that multiple structural characteristics other than contributing area were necessary to explain spatial variability in streamflow. They further provided an excellent example of how structural and hydrologic data, such as water table levels and topographic metrics, can be combined with detailed streamflow data to build an effective field-based and mechanistic view of watershed behavior. However, results from TCEF are not directly comparable, because their study focused on streamflow response to snowmelt and rainfall, where we focused on base flow dynamics over a seasonal recession.

[52] Less direct methods for gathering detailed spatial distribution of streamflow contributions have been suggested using measurements of electrical conductivity [*Appelo et al.*, 1983] or temperature [*Selker et al.*, 2006]. Methods such as these show promise for overcoming the "snapshot bias" problem [*Kuraś et al.*, 2008], in that more rapid or automated flow estimates would minimize temporal bias in spatial snapshots. Distributed measurements of water quality and chemistry, such as these, would also complement distributed discharge measurements in the effort to understand the specific mechanisms behind particular contributions to streamflow.

[53] A common distributed modeling approach to account for spatio-temporal variability in areal yield is to divide the watershed into topographic contributing areas. Then, each contributing area is parameterized such that it generates an independent characteristic flow recession (in the sense of *Harman* et al.[2009]) in response to meteorological drivers [e.g., *Leavesley et al.*, 1983; *Gassman et al.*, 2007]. The spatial distribution of relative flow contributions across TCEF can be interpreted in this context. For example, topographic contributing areas with increasing relative contributions through the summer are also the areas that have lower recession rates. However, this approach is mechanistically invalid if there are times or places where topographically delineated contributing areas do not match the true subsurface contributing areas to streamflow, such as those hypothesized in Figure 8. The recent advent of distributed watershed models with more sophisticated groundwater flow simulation [e.g., *Markstrom et al.*, 2008; *Kollet et al.*, 2010] are capable of accounting for the lack of agreement between topographic slope and subsurface flow direction. The presented data would be a rigorous challenge to the structure of a distributed watershed model of TCEF, thus providing a mechanism to bridge the gap between the experience of the field experimentalist and watershed modeler [*Seibert and McDonnell*, 2002].

[54] Detailed measurements of streamflow along valleys provide the basis for specific identification of stream water sources within watersheds and provide for spatially explicit interpretation of potential structural controls on streamflow generation. These interpretations are necessary to relate the quantity and quality of water in outlet discharge to spatio-temporally variable sources across the watershed, such as in applied efforts to locate and alleviate sources of surface water contaminants to a stream network [e.g., *Kimball et al.*, 2010]. High spatial resolution data are critical to locating boundaries between regions with apparently differing controls on streamflow and subsequently assessing the relative importance of the controls within those boundaries to overall watershed function. Furthermore, changes in the spatial patterns of streamflow through time reveal how the relative influence of various controls on streamflow generation may change with changing discharge conditions.

References

Anderson, M. G., and T. P. Burt (1978), The role of topography in controlling throughflow generation, *Earth Surf. Processes*, *3*(4), 331–344.
Appelo, C. A. J., R. Becht, A. A. Van de Griend, and T. C. M. Spierings (1983), Buildup of discharge along the course of a mountain stream deduced from water-quality routings (EC routings), *J. Hydrol.*, *66*, 305–318.

Baxter, C. V., and F. R. Hauer (2000), Geomorphology, hyporheic exchange, and selection of spawning habitat by bull trout (*Salvelinus confluentus*), *Can. J. Fisheries Aquatic Sci.*, 57, 1470–1481.

Beven, K. (2006), "Commentary," in *Streamflow Generation Processes*, edited by K. Beven, IAHS Press, Wallingford, Oxfordshire, UK.

Beven, K. J. and M. J. Kirkby (1979), A physically based, variable contributing area model of basin hydrology, *Hydrol. Sci. Bull.*, 24(1), 43–69.

Brakensiek, D. L., et al. (1979), Field manual for research in agricultural hydrology, *Agric. Handbook 244*, U.S. Dep. of Agric., Washington, DC.

Day, T. J. (1977), Field procedures and evaluation of a slug dilution gauging method in mountain streams, *J. Hydrol. (N. Z.)*, 16(2), 113–133.

Freer, J., J. J. McDonnell, K. J. Beven, N. E. Peters, D. A. Burns, R. P. Hooper, B. Aulenbach, and C. Kendall (2002), The role of bedrock topography on subsurface storm flow, *Water Resour. Res.*, 38(12), 1269, doi:10.1029/2001WR000872.

Freeze, R. A., and J. A. Cherry (1979), *Groundwater*, Prentice-Hall, Englewood Cliffs, N. J.

Gassman, P. W., M. R. Reyes, C. H. Green, J. G. Arnold (2007), The soil and water assessment tool: Historical development, applications, and future research directions, *Trans. ASABE*, 50(4), 1211–1250.

Genereux, D. P., H. F. Hemond, P. J. Mulholland (1993), Spatial and temporal variability in streamflow generation on the West Fork of Walker Branch Watershed, *J. Hydrol.*, 142(1–4), 137–166.

Gleeson, T., and A. H. Manning (2008), Regional groundwater flow in mountainous terrain: Three-dimensional simulations of topographic and hydrogeologic controls, *Water Resour. Res.*, 44, W10403, doi:10.1029/2008WR006848.

Gooseff, M. N., and B. L. McGlynn (2005), A stream tracer technique employing ionic tracers and specific conductance data applied to the Maimai catchment, New Zealand, *Hydrol. Processes*, 19, 2491–2506.

Harman, C. J., M. Sivapalan, and P. Kumar (2009), Power law catchment-scale recessions arising from heterogeneous linear small-scale dynamics. *Water Resour. Res.*, 45, W09404, doi:10.1029/2008WR007392.

Hewlett, J. D. (1969), *Principles of Forest Hydrology*, Univ. of Ga. Press, Athens.

Huff, D. D., R. V. O'Neill, W. R. Emanuel, J. W. Elwood, and J. D. Newbold (1982), Flow variability and hillslope hydrology, *Earth Surf. Processes Landforms*, 7(1), 91–94.

Jencso, K. G., and B. L. McGlynn (2011), Hierarchical controls on runoff generation: Topographically driven hydrologic connectivity, geology, and vegetation, *Water Resour. Res.*, 47, W11527, doi:10.1029/2011WR010666.

Jencso, K. G., B. L. McGlynn, M. N. Gooseff, S. M. Wondzell, and K. E. Bencala (2009), Hydrologic connectivity between landscapes and streams: Transferring reach- and plot-scale understanding to the catchment scale, *Water Resour. Res.*, 45, W04428, doi:10.1029/2008WR007225.

Jencso, K. G., B. L. McGlynn, M. N. Gooseff, K. E. Bencala, and S. M. Wondzell (2010), Hillslope hydrologic connectivity controls riparian groundwater turnover: Implications of catchment structure for riparian buffering and stream water sources, *Water Resour. Res.*, 46, W10524, doi:10.1029/2009WR008818.

Kimball, B. A., R. L. Runkel, and K. Walton-Day (2010), An approach to quantify sources, seasonal change, and biogeochemical processes affecting metal loading in streams: Facilitating decisions for remediation of mine drainage, *Appl. Geochem.*, 25, 728–740.

Kollet, S. J., R. M. Maxwell, C. S. Woodward, S. Smith, J. Vanderbrought, H. Vereecken, and C. Simmer (2010), Proof of concept of regional scale hydrologic simulations at hydrologic resolution utilizing massively parallel computer resources, *Water Resour. Res.*, 46, W04201, doi:10.1029/2009WR008730.

Kuraś P. K., M. Weiler, and Y. Alila (2008), The spatiotemporal variability of runoff generation and groundwater dynamics in a snow-dominated catchment, *J. Hydrol.*, 352, 50–66.

Larkin, R. G., and J. M. Sharp, Jr. (1992), On the relationship between river-basin geomorphology, aquifer hydraulics, and ground-water flow direction in alluvial aquifers, *Geol. Soc. Am. Bull.*, 104, 1608–1620.

Leavesley, G. H., R. W. Lichty, B. M. Troutman, and L. G. Saindon (1983), Precipitation-runoff modeling system—User's Manual, *U.S. Geol. Surv. Water-Resour. Invest. Rep., 83-4238*, 207 pp., U.S. Geol. Surv., Denver, CO.

Markstrom, S. L., R. G. Niswonger, R. S. Regan, D. E. Prudic, and P. M. Barlow (2008), GSFLOW-Coupled ground-water and surface-water flow model based on the integration of the Precipitation-Runoff Modeling System (PRMS) and the Modular Ground-Water Flow Model (MOD-FLOW-2005), *U.S. Geol. Surv. Tech. Methods*, 6-D1, 240 p.

McGlynn, B. L., J. J. McDonnell, J. Seibert, and M. K. Stewart (2003), On the relationships between catchment scale and streamwater mean residence time, *Hydrol. Processes*, 17, 175–181.

McGuire, K. J., J. J. McDonnell, M. Weiler, C. Kendall, B. L. McGlynn, J. M. Welker, and J. Seibert (2005), The role of topography on catchment-scale water residence time, *Water Resour. Res.*, 41, W05002, doi:10.1029/2004WR003657.

Mincemoyer, S. A., and J. L. Birdsall (2006), Vascular flora of the Tenderfoot Creek Experimental Forest, Little Belt Mountains, Montana, *Madroño*, 53(3), 211–222.

Montgomery, D. R. (1999), Process domains and the river continuum, *J. Am. Water Resour. Assoc.*, 35(2), 397–410.

O'Callaghan, J. F., and D. M. Mark (1984), The extraction of drainage networks from digital elevation data, *Comput. Vision Graphics Image Process.*, 28(3), 323–344.

Payn, R. A., M. N. Gooseff, B. L. McGlynn, K. E. Bencala, and S. M. Wondzell (2009), Channel water balance and exchange with subsurface flow along a mountain headwater stream in Montana, United States, *Water Resour. Res.*, 45, W11427, doi:10.1029/2008WR007644.

Poole, G. C., J. A. Stanford, C. A. Frissell, and S. W. Running (2002), Three-dimensional mapping of geomorphic controls on flood-plain hydrology and connectivity from aerial photos, *Geomorphology*, 48, 329–347.

Reynolds, M. (1995), Geology of Tenderfoot Creek Experimental Forest, Little Belt Mountains, Meagher County, Montana., in *Hydrologic and Geologic Characteristics of Tenderfoot Creek Experimental Forest, Montana, Final Rep. RJVA-INT-92734*, edited by P. Farnes, et al. pp. 21–32, U.S. Dep. of Agric., Bozeman, MT.

Reynolds, M. W., and T. R. Brandt (2007), Preliminary geologic map of the White Sulphur Springs 30' × 60' quadrangle, Montana, *U.S. Geol. Surv. Open-File Rep., 2006-1329*, scale 1:100:000, 1 p., U.S. Geol. Surv., Denver, CO.

Seibert, J., and J. J. McDonnell (2002), On the dialog between experimentalist and modeler in catchment hydrology: Use of soft data for multicriteria model calibration, *Water Resour. Res.*, 38(11), 1241, doi:10.1029/2001WR000978.

Seibert, J., and B. L. McGlynn (2007), A new triangular multiple flow-direction algorithm for computing upslope areas from gridded digital elevation models, *Water Resour. Res.*, 43, W04501, doi:10.1029/2006WR005128.

Selker, J., N. Van de Giesen, M. Westhoff, W. Luxemburg, and M. B. Parlange (2006), Fiber optics opens window on stream dynamics, *Geophys. Res. Lett.*, 33, L24401, doi:10.1029/2006GL027979.

Sivapalan, M., et al. (2003), IAHS decade on Predictions in Ungauged Basins (PUB), 2003–2012: Shaping an exciting future for the hydrological sciences, *Hydrol. Sci. J.*, 48(6), 857–880.

Stanford, J. A., and J. V. Ward (1993), An ecosystem perspective of alluvial rivers: connectivity and the hyporheic corridor, *J. N. Am. Benthol. Soc.*, 12(1), 48–60.

Tóth, J. (1963), A theoretical analysis of groundwater flow in small drainage basins, *J. Geophys. Res.*, 68, 4795–4812.

Uchida, T., S. Miyata, and Y. Asano (2008), Effects of the lateral and vertical expansion of the water flowpath in bedrock on temporal changes in hillslope discharge, *Geophys. Res. Lett.*, 35, L15402, doi:10.1029/2008GL034566.

Wondzell, S. M. (2006), Effect of morphology and discharge on hyporheic exchange flows in two small streams in the Cascade Mountains of Oregon, USA, *Hydrol. Processes*, 20(2), 267–287.

Wörman, A., A. I. Packman, L. Marklund, J. W. Harvey, and S. H. Stone (2007), Fractal topography and subsurface water flows from fluvial bedforms to the continental shield, *Geophys. Res. Lett.*, 34, L07402, doi:10.1029/2007GL029426.

Zellweger, G. W., R. J. Avanzino, and K. E. Bencala (1989), Comparison of tracer-dilution and current-meter discharge measurements in a small gravel-bed stream, Little Lost Man Creek, California, *U.S. Geol. Soc. Water-Resour. Invest. Rep., 89-4150*, 20 pp., U.S. Geol. Surv., Menlo Park, CA.

K. E. Bencala, U. S. Geological Survey, 345 Middlefield Rd., MS439, Menlo Park, CA 94025, USA.

M. N. Gooseff, Department of Civil and Environmental Engineering, Pennsylvania State University, University Park, PA 16802, USA.

B. L. McGlynn and R. Payn, Department of Land Resources and Environmental Sciences, Montana State University, PO Box 173120, MT 59717-3120, Bozeman, USA. (rpayn@montana.edu)

S. M. Wondzell, Pacific Northwest Research Station, United States Department of Agriculture Forest Service, 3200 SW Jefferson Way, Corvallis, OR 97331, USA.